Resonant Raman scattering in ZnO

J. M. Calleja* and Manuel Cardona
Max-Planck-Institut für Festkörperforschung, 7000 Stuttgart 80, Federal Republic of Germany
(Received 19 May 1977)

The resonance of the Raman scattering by E_2, A_{1T}, E_{1L}, and E_{1T} phonons, and several second-order features, has been studied for ZnO for photon energies between 1.6 and 3 eV. The results are interpreted with a dielectric theory based on the first and second derivatives of the dielectric constant. By combining our results with absolute scattering cross sections previously determined by Arguello *et al.* at 2.41 eV absolute values of the deformation potentials of the band edge can be determined. The difference in strength between the longitudinal and the transverse modes provides the signs of these deformation potentials. The antiresonance around 1.6 eV suggested by the earlier work of Callender *et al.* and attributed to a cancellation of the deformation potential and electro-optical contributions to the Raman tensor is confirmed. The deformation potentials of the A_1 phonons at the band edge have been obtained from a pseudopotential calculation. While the sign of these deformation potentials agrees with the experimental determination, their magnitudes do not agree. This fact is attributed to difficulties with the pseudopotential of the O^{2-} ion. An estimate of the deformation potentials from the dependence of the band edges on uniaxial stress is also made.

I. INTRODUCTION

ZnO, the mineral zincite, crystallizes in the wurtzite structure (space group C_{6v}^4) which possesses four atoms per primitive cell.[1] The dispersion relations of phonons (and also of electrons) along the Δ direction (hexagonal axis) can be approximately derived by folding those of the corresponding zinc-blende crystal (two atoms per primitive cell) along the [111] direction.[2] Thus one finds at $\vec{k}=0$ (Γ) two sets of infrared- and Raman-active modes, A_1 (singlet) and E_1 (doublet), which correspond to the optical modes of zinc-blende.[3,4] Besides, as a result of the folding, additional infrared-inactive modes appear at Γ, as shown in Fig. 1. They are two sets of E_2, Raman-active doublet modes and two Raman-inactive singlets (B). Raman A_1, E_1, and E_2 modes have been recently observed by Arguello *et al.*[3] and identified according to their polarization selection rules. The infrared-active E_1 and A_1 modes can be seen to split into E_{1L} and A_{1T} (L, longitudinal; T, transverse) for propagation perpendicular to the c axis and E_{1T}, A_{1L} for parallel propagation as a result of the polarization which accompanies longitudinal infrared-active excitations.[5] For propagation at an angle other than 0° or 90° to the c axis mixed modes are obtained. Neutron-scattering data, confined mainly to the low-frequency branches of the dispersion curves, have recently complemented our knowledge of the lattice dynamics of ZnO,[4,6] and provided a basis for parametrized calculations such as that shown in Fig. 1.

In spite of the interest in ZnO and of a considerable number of calculations,[7,8] the knowledge of its electronic bands is rather imperfect except for the details of the lowest band edge at $\vec{k}=0$ (which is usually used as an experimental fitting parameter for calculations!). The Korringa-Kohn-Rostoker (KKR) calculations[7] yield the wrong position for the $3d$ core levels of the Zn while the empirical pseudopotential work[8] is not able to reproduce the details of the optical-absorption spectrum, a fact believed due to difficulties in setting up a local pseudopotential for O^{2-}.

However, the experimental picture concerning the lowest direct edge (actually excitons) seems clear. At room temperature there is an edge at 3.32 eV polarized perpendicular to the c axis, (A, B) with a parallel polarized counterpart (C) at 3.36 eV.[9] The (A, B) exciton exhibits a very small negative spin-orbit splitting[10] which only becomes observable at low temperatures. The A, B, and C excitons correspond to the so-called E_0 edge. Note that the E_0 edge in ZnO is smaller than that of ZnS (3.7 eV),[11] a fact which has thus far escaped theoretical understanding. The Raman-scattering efficiencies are expected to resonate when the laser frequency approaches E_0. These resonances have been investigated for a number of zinc-blende-type semiconductors.[12] They can be used to study the details of the scattering mechanism and to determine electron-phonon coupling constants or deformation potentials. Work of this sort for ZnO has been rather limited because of the awkwardness, from the point of view of laser technology, of the region in which E_0 occurs (3.3 eV = 3750 Å). A study[13] at 4.2° K of the Fröhlich-interaction-induced $2E_{1L}$ scattering, using a pulsed dye laser in the region from 3.28 to 3.36 eV, has been published but unfortunately this type of scattering is difficult to in-

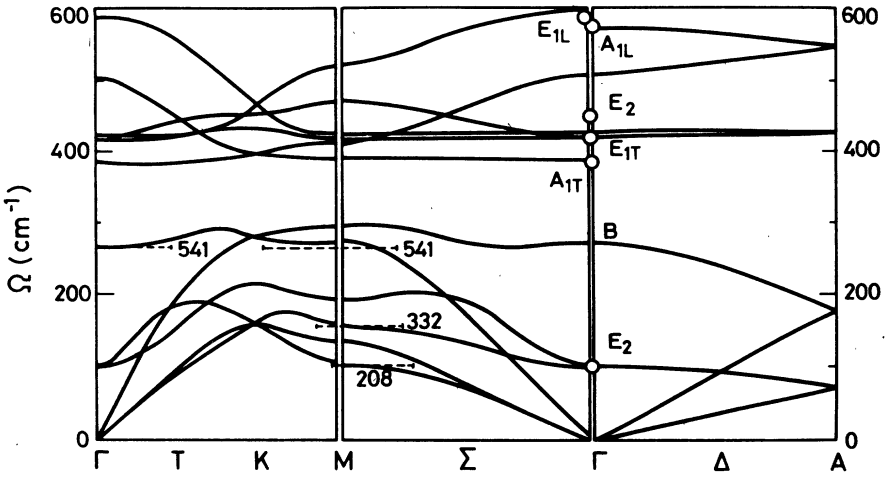

FIG. 1. Phonon dispersion relations for ZnO at room temperature taken from Ref. 4. The points indicate the phonon frequencies determined by Raman scattering (Ref. 21); the dashed bars represent a tentative assignment of the second-order structures shown in Fig. 2(a).

terpret quantitatively.[14] A study of the E_{1L}, E_{1T}, A_{1T}, and E_2 resonances in the energy range 1.92–2.57 eV has appeared more recently.[15] While this range is still quite far from the E_0 edge of ZnO one can already identify in it resonance effects. In fact, by extrapolation of the observed E_{1L} resonance the data of these authors suggest the existence of an antiresonance in the scattering by E_{1L} phonons at about 1.6 eV. They attribute this behavior to a destructive interference between deformation potential and interband Fröhlich interaction (i.e., electro-optic effect) scattering.

In this paper we investigate resonance Raman scattering of all modes mentioned above for ZnO plus a few second-order structures at room temperature in the 1.6–3 eV region which approaches sufficiently the E_0 edge to clearly distinguish resonance effects. On the low-photon-energy side our experimental region reaches the energy of the suspected E_{1L} antiresonance and we are thus able to confirm its existence. In Sec. II we discuss the experimental details. In Sec. III we present the experimental data and we fit them with expressions based on derivatives of the dielectric constant.

By normalizing to the values of absolute scattering efficiencies given in Ref. 3 for 2.41 eV it is possible to present our data as absolute efficiencies. In Sec. IV we discuss the results in terms of deformation potentials and electrooptic coefficients. We present the results of a pseudopotential calculation of the deformation potentials of the A_1 modes for the E_0 gap of ZnO. While this calculation predicts the sign of the deformation potentials extracted from our Raman data (by comparison to the sign of the electro-optic coefficients[16]) the calculated magnitudes do not agree with experiment.

We also make an estimate of the A_1, E_1, and E_2 deformation potentials from the observed dependence of the E_0 gap on uniaxial stress along several directions.[17]

II. EXPERIMENTAL DETAILS

The measurements were performed at room temperature on a $2\times2\times10$ mm ZnO single crystal with all faces polished and the long dimension along the c axis. We tried to etch the crystal with phosphoric acid, but such procedure, as well as the use of cleaved surfaces, resulted, for frequencies above the gap, in a strong luminescence which largely obliterated our Raman spectra. Since the measurements discussed here are confined to a region in which the crystal is transparent we do not think etching is necessary. The x and y axes were perpendicular to two long faces; a distinction between x and y is not necessary for our work. The symmetries of Raman active phonons and the corresponding Raman tensors for the C_{6v} point group are[5]

$$A_1(Z)\rightarrow\begin{pmatrix} a & & \\ & a & \\ & & b \end{pmatrix};\quad \begin{cases} E_1(Y)\rightarrow\begin{pmatrix} 0 & 0 & 0 \\ 0 & 0 & c \\ 0 & c & 0 \end{pmatrix} \\ E_1(X)\rightarrow\begin{pmatrix} 0 & 0 & c \\ 0 & 0 & 0 \\ c & 0 & 0 \end{pmatrix} \end{cases};$$

$$\begin{cases} E_2^{(1)}\rightarrow\begin{pmatrix} d & 0 & 0 \\ 0 & -d & 0 \\ 0 & 0 & 0 \end{pmatrix} \\ E_2^{(2)}\rightarrow\begin{pmatrix} 0 & d & 0 \\ d & 0 & 0 \\ 0 & 0 & 0 \end{pmatrix} \end{cases} \qquad (1)$$

The A_1 and E_1 phonons are infrared active and hence they split into transverse and longitudinal modes ($A_{1L}, A_{1T}, E_{1L}, E_{1T}$). There are therefore two independent sets of Raman tensor components a, b, and c ($a_L, a_T, b_L, b_T, c_L, c_T$). The scattering geometries used in our experiments, the corresponding phonons, and the scattering efficiencies S in terms of the parameters of Eq. (1) are (in standard notation)

$$x(zz)\bar{x} \to A_{1T};\quad S=b_T^2$$
$$x(zx)y \to E_{1T}, E_{1L};\quad S=\tfrac{1}{2}c_T^2, \tfrac{1}{2}c_L^2 \qquad (2)$$
$$x(yy)x \to A_{1T}, E_2;\quad S=a_T^2, d^2\ .$$

The purpose of the present work is to determine the dependence of a_T, b_T, c_T, c_L, and d on exciting wavelength and to interpret this dependence theoretically. We found no convenient configuration yielding the parameters a_L or b_L (see Refs. 3 and 15).

The spectra were excited with all the lines of Spectra Physics models 164, 165, and 185 lasers (Ar^+, Kr^+, and He-Cd, respectively) and analyzed by means of a $\frac{3}{4}$-m SPEX double monochromator with Jobin-Yvon holographic gratings (1800 lines/mm) and a RCA C-31034A photomultiplier. The data were then corrected in the usual way (by comparison with the scattering from a CaF_2 crystal) for the throughput function of the spectrometer and the ω^4 factor so as to obtain data which can be related to the square of the transition susceptibility or Raman tensor.[12] Corrections for the absorption and the reflectivity[18-20] were only needed for the data at 4067 Å (3.05 eV); they changed the scattering efficiencies by only 20%.

III. RESULTS

Typical spectra obtained with 4880 Å (2.54 eV) excitation wavelength are shown in Figs. 2(a)–2(c) for the three configurations of Eq. (2), respectively. These spectra agree basically with those reported earlier.[3,21] The arrows in Figs. 2(a)–2(c) indicate the position of the phonons and two-phonon structures whose resonance is shown in Figs. 3–5. In addition to the phonons shown in Fig. 2 we observed for 4067-Å laser excitation the E_{1L} phonon in the forbidden configuration $x(zz)\bar{x}$. This is a standard occurrence for ir-active phonons which is believed to be due to intraband Fröhlich interaction.[12] Similarly, we detected for this wavelength a weak A_{1L} phonon at 574 cm^{-1} in the $z(xx)\bar{z}$ allowed configuration. We were not able to see this phonon at longer wavelengths.

We have also performed some measurements with the 3638 Å (3.41 eV, Ar^+), 3507 Å (3.53 eV, Kr^+), and 3250 Å (3.82 eV, HeCd) laser lines. In

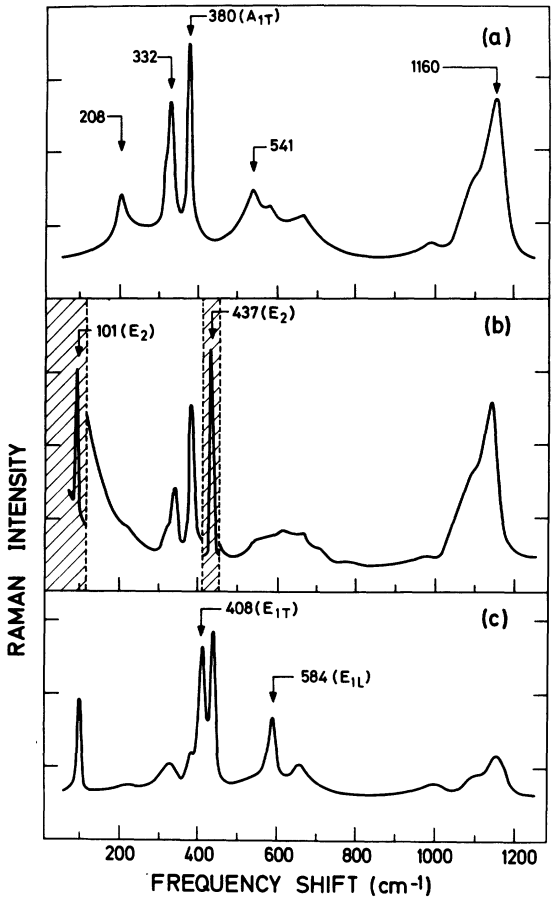

FIG. 2. Raman spectra recorded at room temperature with 4880-Å excitation wavelength for the $x(zz)\bar{x}$ (a), $x(yy)\bar{x}$ (b), and $x(zx)y$ (c) configurations. The arrows indicate the position of the one-phonon and two-phonon structures whose resonance is presented in Fig.s 4–6. In the shadowed regions of (b) the Raman intensity has been divided by 2.

all these cases we observed, like in previous works,[15,22] up to six overtones of the E_{1L} phonon of intensity decreasing with increasing order and independent of polarization configuration. This last fact may be due to the poor quality of the polished surfaces and the strong absorption coefficient in this region ($\gtrsim 10^5$ cm^{-1}). However, we saw in this region no traces of the A_{1L} mode or its overtones in spite of having seen it for 4067-Å excitation.

In Fig. 3 spectra similar to those of Fig. 2(a) are presented for several exciting wavelengths. It is worth noting that the $2E_{1L}$ peak is resonantly enhanced with respect to the rest of the spectrum already at photon energies ~1 eV below E_0. More details about the $2E_{1L}$ resonance can be found in Refs. 13 and 23.

The integrated scatterering efficiencies observed for the two E_2 phonons [d^2 coefficients of

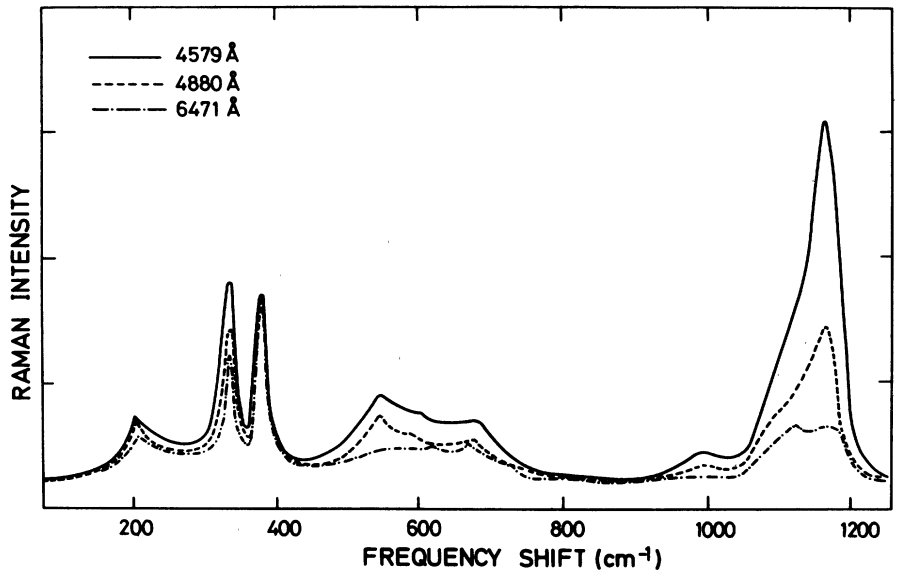

FIG. 3. Raman spectra recorded for several wavelengths in $x(zz)\bar{x}$ configuration. Note the nearly constant A_{1T} height and the strong resonance of the 2LO region.

Eq. (2)] and for the A_{1T} phonon (a_T^2 coefficient) are plotted in Fig. 4 as a function of photon energy. Absolute values of these scattering coefficients (in units of $cm^{-1}sr^{-1}$) are given; they were obtained by normalizing our data to the absolute scattering cross sections measured by Arguello *et al.*[3] at 2.41 eV for the a_T^2 coefficient of the A_{1T} phonon. Note, however, that the ω^4 factor has been re-

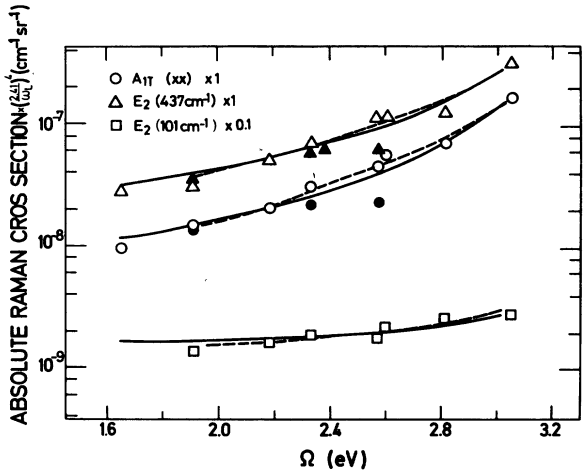

FIG. 4. Absolute Raman efficiency vs exciting frequency for the $A_{1T}(xx)$ (○), E_2 (437 cm^{-1}) (△), and E_2 (101 cm^{-1}) (□) phonons obtained in $x(yy)\bar{x}$ configuration. The full symbols (●, ▲, ■) represent data taken from Ref. 15. The results have been normalized to the absolute values of the Raman cross section for $\omega = 2.41$ eV given in Ref. 3. Note that the ω dependence has been removed and thus the absolute values of the cross section in the sense of Eq. (8) are obtained by multiplying the strengths shown in the figure by $(\omega/2.41)^4$. This also holds for Figs. 5 and 6. The dashed and solid lines are the least-squares fit to our data with Eqs. (3) and (4), respectively. The corresponding values of the A, B, A' and B' coefficients are listed in Table I.

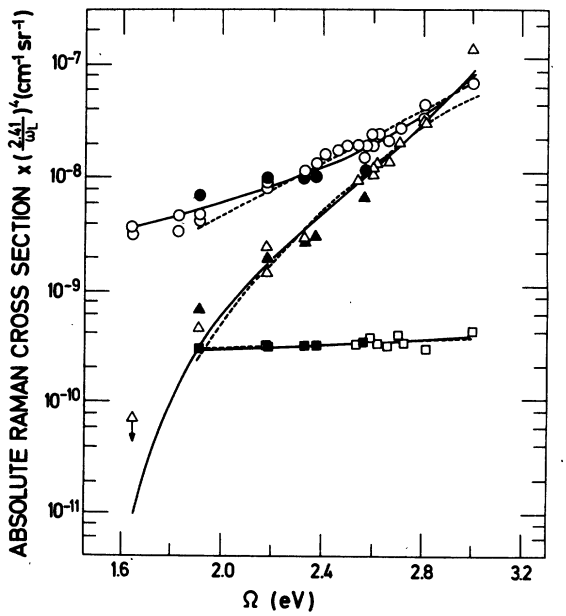

FIG. 5. Absolute Raman efficiency vs exciting wavelength for E_{1T}(○) and E_{1L} (△) phonons in $x(zx)y$ configuration and for $A_{1T}(zz)$ (□) in $x(zz)\bar{x}$ configuration. (Note that the $A_{1T}(zz)$ data are shifted two decades downwards for display purposes.) The dashed and solid lines are again the fits of Eqs. (3) and (4), respectively. The full symbols (●, ▲, ■) are data taken from Ref. 15. The triangle marked with an arrow is an upper-limit estimate of the E_{1L} Raman cross section at 1.65 eV.

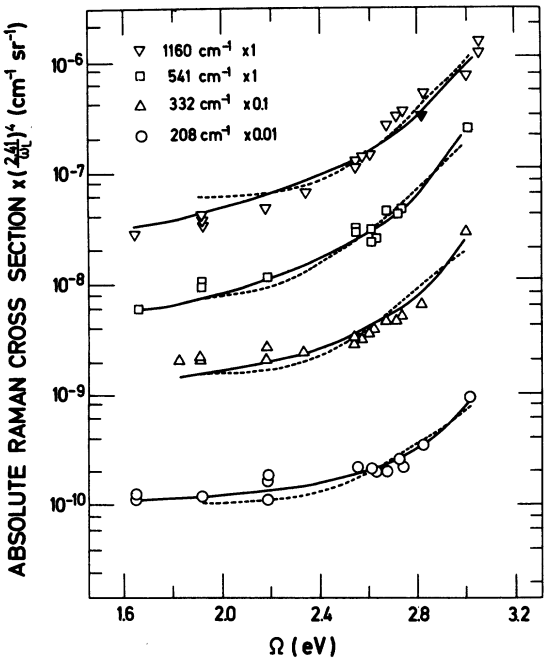

FIG. 6. Absolute Raman efficiency vs exciting wavelength for the second-order structures shown in Fig. 2(a) in $x(zz)\bar{x}$ configuration. The full triangle has been taken from Ref. 23. The dashed and solid lines are the least-squares fit to the data with Eqs. (6) and (7), respectively. The corresponding C, C', D and D' coefficients are listed in Table I. The ordinate scales of the different curves have been shifted for display purposes.

moved from the scattering efficiency of Figs. 4–6. The experimental points of Ref. 15, also renormalized in this manner, have been included in Fig. 4. They show substantial agreement with our data except for a slightly smaller slope.

The dashed lines in Fig. 4 represent a least-squares fit to the experimental scattering efficiencies I with the expression

$$I=A\left(\frac{d\epsilon}{d\omega}+B\right)^2, \tag{3}$$

which is based on the dielectric theory (see Sec. IV). The frequency derivative of the dielectric constant (in eV^{-1}) has been obtained by differentiating the data of Refs. 24 and 25. The constant B represents a nonresonant contribution to the Raman tensor. The values of A and B required for the fits are given in Table I. We have also performed a fit to the data of Fig. 4 (solid line) with the expression

$$I=A'[-g(x)+B']^2$$

with

$$g(x)=x^{-2}[2-(1-x)^{1/2}-(1+x)^{-1/2}] \tag{4}$$

and

$$x=\omega/\omega_0\ ,$$

ω_0 being the frequency of the E_0 gap. The function $g(x)$ is one of a family of functions used in the theory of dielectric properties of three-dimensional energy bands extending to infinity.[26,27] It represents the derivative of the dielectric constant with respect to the energy gap ω_0 under the assumption of a density of states mass independent of ω_0.[27] This function is used often to represent the resonance of the first-order Raman tensor near three-dimensional critical points.[27] It is easy to show within the model of parabolic bands that for ω close to but below ω_0 the following equation holds:

TABLE I. Coefficients resulting from the least-squares fit to the experimental Raman cross sections with Eqs. (3), (4), (6), and (7). A and A' have been normalized so as to obtain at 2.41 eV the absolute cross sections given in Ref. 3. Units are 10^{-8} $eV^2cm^{-1}sr$ for A, 10^{-8} $cm^{-1}sr^{-1}$ for A' and C', eV^{-1} for B, 10^{-8} $eV^4cm^{-1}sr$ for C, and eV^{-2} for D. B' and D' are dimensionless. For the purpose of comparison with B we have tabulated $B'+\frac{3}{4}$ instead of B' [see Eqs. (4) and (5)].

First order	A	B	A'	$B'+\frac{3}{4}$
a_T^2	1.86	0.66	3.85	0.34
b_T^2	0.02	12.02	0.03	9.31
c_T^2	1.45	0.28	2.03	0.24
c_T^2	1.25	−0.08	3.03	−0.15
d^2 (437 cm^{-1})	2.94	0.90	6.96	0.49
d^2 (101 cm^{-1})	0.07	4.46	0.09	4.05
Second order	C	D	$C'\times10^2$	$D'+1$
208 cm^{-1}	0.54	0.31	0.39	14.17
332 cm^{-1}	2.15	−0.24	1.70	6.80
541 cm^{-1}	2.50	−0.50	1.90	3.68
1160 cm^{-1}	7.77	−0.22	6.30	6.63

$$\frac{d\epsilon}{d\omega} \simeq -K[g(x)+\tfrac{3}{4}]. \tag{5}$$

While ZnO has strong excitons at E_0, the parabolic bands expression [Eq. (5)] should be valid in our experimental region ($x \lesssim 0.9$) as can be seen by examining Eqs. (58) and (60) of Ref. 26. The value of K^2 evaluated from the mass parameters of ZnO is 0.6,[26] in reasonable agreement with the ratio of A and A' shown in Table I.

The resonance in the scattering efficiencies of the E_{1L} (c_L^2), E_{1T} (c_T^2), and A_{1T} (b_T^2) phonons is shown in Fig. 5. The absolute cross sections were determined by fitting to the measurements of Ref. 3 at 2.41 eV. Fits with Eqs. (3) and (4) are also represented in this figure, which includes the data of Ref. 15, by dashed and solid lines, respectively. The efficiencies of E_{1L} at 1.65 and 3.05 eV have not been included in our fit since they are affected by considerable uncertainty. In fact, the E_{1L} point at 1.65 eV, indicated by an arrow, is only an upper limit for the Raman cross section, since we could not detect any signal in that case. Our data for E_{1L} clearly indicate the existence of an antiresonance at ~1.6 eV, corresponding to a cancellation of the resonant and nonresonant terms in Eqs. (3) and (4). The A_{1T} mode hardly shows any resonance at all; the corresponding values of the resonating terms are zero within the experimental uncertainty.

In Fig. 6 we present the resonance behavior of the main second-order structures of Fig. 2, the $2E_{1L}$ structure at 1160 cm^{-1} and the weaker structures at 541, 332, and 208 cm^{-1}. Since these features seem to resonate more strongly than their first-order counterparts (except for the behavior of the E_{1L} mode in Fig. 4 which can only be explained as an antiresonance), we have chosen to fit them with the second derivatives of the dielectric constant

$$I = C\left(\frac{d^2\epsilon}{d\omega^2}+D\right)^2 \tag{6}$$

or, corresponding to Eq. (4),

$$I = C'[(1-x)^{-3/2}+D']^2. \tag{7}$$

We have left in Eq. (7) only the most dispersive part of the derivative of $g(x)$. The parameters C, C', D, and D' required for the fits of Fig. 6 are also given in Table I.

IV. DISCUSSION

We have already mentioned that Eqs. (3), (4), (6), and (7), which have been used to fit the experimental resonance data, are based on the dielectric theory of Raman scattering. This theory contains several assumptions:

(a) The phonon frequency Ω is always much smaller than $\omega - \omega_0$ (ω is the laser frequency, ω_0 that of the E_0 gap) so that the phonon can be treated as a quasistatic perturbation. Under this assumption it is easy to see that the efficiency for Stokes scattering per unit length and unit solid angle is given, in units of sr^{-1} bohr^{-1}, by[12]

$$\sigma_i(\omega) = \left(\frac{\omega}{c_0}\right)^4 \left|\frac{\partial \chi_{jk}}{\partial u_i}\right|^2 |\langle n_i+1|u_i|n_i\rangle|^2, \tag{8}$$

where j and k are the directions of the incident and scattering fields, χ the susceptibility tensor, u_i the atomic displacements associated with the ith phonon, n_i, its Bose occupation number, and c_0 the speed of light in vacuum. Equation (8) is written in atomic units (i.e., $e=\hbar=m=1$, $c_0=137$).

(b) We assume that $\partial\chi_{jk}/du_i$ has two contributions, a strongly dispersive one arising from the lowest gap E_0 and a contribution from all higher gaps, represented by B and B', which is nearly constant below E_0. The E_0 contribution can also be split into two components. The most strongly dispersive of these components originates from a modulation of the E_0 gap (or any of its three components A, B, C) by the phonon displacement u_i. This type of contribution exists for the A_{1T} (this phonon modulates the conduction and all the valence bands which have E_1 symmetry). The other type of contribution is usually less dispersive very near the gap. It corresponds to changes in the transition matrix elements due to interband mixing of wave functions. To this type belongs the effect of the E_{1T} phonon which couples the A, B valence bands with the C band. Both types of effects which occur in ZnO cannot be distinguished if the three valence bands are degenerate, i.e., if $\omega_{AC} \simeq 0$, or equivalently if $\omega_{AC} \ll \omega_0 - \omega$ for the experimental region of interest. This condition is well fulfilled in our case ($\omega_0 - \omega \gtrsim 0.3$ eV, $\omega_{AC} = 0.036$ eV) and therefore we only have one type of E_0 contribution which can be written in terms of derivatives of χ with respect to energy gaps:

$$\frac{\partial \chi_{jk}}{\partial u_i} = \frac{\partial \chi_{jk}}{\partial \omega_0}\frac{\partial \omega_0}{\partial u_i} \simeq -\frac{\partial \chi_{jk}}{\partial \omega}\frac{\partial \omega_0}{\partial u_i}. \tag{9}$$

The replacement of $d\chi_{jk}/d\omega_0$ by $-d\chi_{jk}/d\omega$ in Eq. (9) strictly speaking requires the addition of a less dispersive function which is omitted since it can be lumped into the constants B and B'.

The dispersionless background B (or equivalently B') is dominant for the A_{1T} mode in (zz) configuration [b_T^2 coefficient of Eq. (2)]; in this case the resonant term is nearly zero within the experimental error. The background is also large for the E_2 mode although in this case a resonant contribution clearly exists.

We now proceed to give explicit expressions for the A's of the various Stokes modes in terms of

electron-phonon interaction constants or deformation potentials, i.e., of derivatives of the energies of the various states forming the gap with respect to the phonon displacements u_i. Using Eqs. (3), (8), and (9), we can write

$$A=\frac{n_i+1}{16\pi^2c_0^4}\langle u_i^2\rangle\left|\frac{\partial\omega_0}{\partial u_i}\right|^2, \tag{10}$$

where $\langle u_i^2\rangle^{1/2}$ is the zero-point vibration amplitude of the phonon under consideration and n_i the Bose-Einstein factor. For A_1 phonons we take as $u(A_1)$ the change in length of a ZnO bond parallel to the c axis. It is then customary to introduce the dimensionless parameter $\delta(A_1)$ which is the vibration amplitude divided by the bond length $\frac{3}{8}c$ (c and a are the lattice constants). We thus find

$$A(A_{1T})=\frac{\sqrt{3}(n(A_{1T})+1)a^2}{18\pi^2c_0^4\mu c\Omega(A_{1T})}\left|\frac{\partial\omega_0}{\partial\delta(A_1)}\right|^2, \tag{11}$$

where μ is the reduced mass of the Zn and O atoms. (Note that Eq. (8) has the explicit ω^4 dependence, whereas in Figs. 4–6 and in Eqs. (3)–(7) this dependence has been removed by normalizing our data to the absolute cross sections given in Ref. 3 for $\omega=2.41$ eV. Thus, for using the A's of Table I in Eqs. (11)–(13), they must be multiplied by $(27.2/2.41)^4$, 27.2 being the factor to convert eV to hartree, and by 5.3×10^{-9} in order to convert cm^{-1} to atomic units.) For the E_1 mode the vibration is perpendicular to the c axis. We thus use as a normalization for $u(E_1)$ the component of an oblique Zn–O bond perpendicular to this axis $(a/\sqrt{3})$. We obtain

$$A(E_{1T})=\frac{3\sqrt{3}(n(E_{1T})+1)c}{128\pi^2c_0^4\mu\Omega(E_{1T})}\left|\frac{\partial\omega_v}{\partial\delta(E_{1T})}\right|^2, \tag{12}$$

where $\partial\omega_v$ represents the matrix element of the electron-phonon interaction between the A and the C valence-band states.

For the E_2 modes an additional complication arises due to the fact that there are two modes of this type. Thus their eigenvectors are not determined by symmetry, but by the solution of the corresponding dynamical matrix. However, since they are well separated in frequency (101 and 437 cm^{-1}) it is reasonable to assume that the low-frequency mode is due exclusively to vibrations of the heavy Zn sublattice while that at 437 cm^{-1} involves only oxygen vibrations. This fact explains why the low-frequency E_2 mode does not resonate at E_0: The vibrations of the zinc sublattice do not modulate much the A, B, and C valence-band states of ZnO, composed almost exclusively of oxygen $2p$ wave functions. We thus write for the E_2 (437 cm^{-1}) mode the expression

$$A[E_2(437\ \mathrm{cm}^{-1})]=\frac{3\sqrt{3}(n(E_2)+1)c}{32\pi^2c_0^4M\Omega(E_2)}\left|\frac{\partial\omega_v}{\partial\delta(E_2)}\right|^2, \tag{13}$$

where $\partial\omega_v$ represents the matrix element of the electron-phonon interaction between the A and the B valence bands and M is the mass of the oxygen atoms. A similar equation could be written for the E_2 (101 cm^{-1}) mode. The derivatives in Eqs. (11)–(13) shall be referred to as the deformation potentials $d_0(A_1)$, $d_0(E_1)$, and $d_0(E_2)$, respectively. The values of these deformation potentials obtained from the A's of Table I with Eqs. (11)–(13) are listed in the first column of Table II. There are two deformation potentials for A_1, one in the (xx) configuration corresponding to a_T^2 of Eq. (2) and another for the (zz) configuration corresponding to b_T^2. As already expected, $d_0[A_1(zz)]\approx0$. It is not possible to determine from our data for *transverse* phonons the sign of d_0. This sign can be determined for the ir-active phonons by analyzing the strength of the corresponding longitudinal modes.[15] In fact, the A's for these modes contain instead of $|d_0|^2$ the square of a linear combination of d_0 and the corresponding electro-optic coefficient d_{ijk}. Since the signs and magnitudes of these d_{ijk} are known,[15,16] one can in this manner determine the

TABLE II. Deformation potentials for ZnO in eV corresponding to the $A_{1T}(xx)$, $A_{1T}(zz)$, E_{1T}, and E_2 phonons. The first column contains the values obtained from the A's of Table I and Eqs. (11)–(13). The signs have been evaluated (Ref. 15) from the electro-optic coefficients given in Ref. 16 for the A_{1T} and E_{1T} phonons. The values obtained from Eq. (14) and the results of the pseudopotential calculations are listed in the second and third columns, respectively.

	From resonant Raman work	From piezo-optical work	Pseudopotential calculation
$A_{1T}(xx)$	+0.73	+1.84	+1.41
$A_{1T}(zz)$	−0.07	−0.02	−4.39
E_{1T}	−0.66	−2.12	•••
E_2 (437 cm^{-1})	0.54	+1.2	•••
E_2 (101 cm^{-1})	0.05	•••	•••

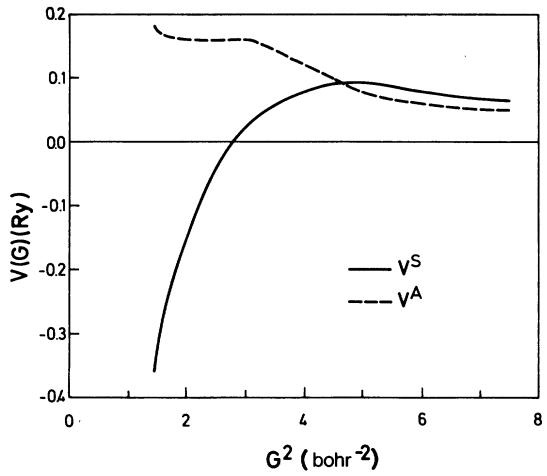

FIG. 7. Pseudopotential form factors v^A and v^S (in rydbergs) for ZnO obtained from Ref. 35, vs the square of the reciprocal-lattice vector (G).

signs of $d_0(A_1)$ and $d_0(E_1)$. The signs so determined[15] are given with the experimental data in the first column of Table II. We have made an attempt to calculate $d_0[A_1(xx)]$ and $d_0[A_1(zz)]$ with the pseudopotential method.[8] This calculation is particularly simple since the A_1 phonons preserve the symmetry of the crystal: this is not the case for the E_1 and E_2 phonons. The results of this calculation, performed with the pseudopotential form factors of Fig. 7, are given in the third column of Table II. The calculation predicts the signs of d_0 observed experimentally, but fails to reproduce the nearly vanishing $d_0[A_1(zz)]$. We believe this is due to inadequacies with a local pseudopotential for the O^{2-} ion. This ion has no p-core states and hence the corresponding pseudopotential cannot be smooth near the core. We have thus made an attempt to relate the d_0's to the deformation potentials $C_1, \ldots, C_6$ obtained in Refs. 17 and 28 for ZnO under uniaxial stress. A connection between both types of deformation potentials can be made by noting that upon application of a uniaxial stress the unit cell of wurtzite does not deform uniformly but there are additional relative displacements of the various atoms. Hence the effect of the stress can be decomposed into a uniform deformation of the unit cell plus various phonons producing the relative displacements.[27] It has been noted[27] that for zinc-blende-type crystals the effect of a [111] stress on the valence bands at Γ is produced *exclusively* by the phonon component. By making the same assumption for ZnO and assuming also that the bonds do not change length upon uniaxial deformation,[29] it is possible to relate the C_i's to the d_0:

$$
\begin{aligned}
d_0[A_1(xx)] &= -(C_1+C_3)+2\frac{S_{13}}{S_{33}}(C_2+C_4)-\frac{1}{3S_{33}}C_\perp^h,\\
d_0[A_1(zz)] &= -\left(C_1+\frac{2S_{13}}{S_{33}}C_2-\frac{1}{3S_{33}}C_\parallel^h\right),\\
d_0(E_1) &= -3C_6/2\sqrt{2},\\
d_0(E_2) &= C_5,
\end{aligned}
\tag{14}
$$

where S_{13} and S_{33} are the elastic compliance constants[33] and $C_\perp^h, C_\parallel^h$ the hydrostatic stress deformation potentials for the (A,B) and C excitons, respectively, taken from data of Ref. 34.

The values of the d_0's obtained from Refs. 17 and 28 with Eqs. (14) are listed in the second column of Table II. Their signs agree with the experimentally determined ones. The $d_0[A_1(zz)]$ so calculated is very small, in agreement with the experimental value. The other d_0's so obtained are larger than the experimental ones. In spite of the crudeness of our assumptions this raises the possibility of a systematic error in the absolute efficiency measurements of Ref. 3. Much better agreement with the various deformation potential calculations would be obtained if the measured efficiencies were about one order of magnitude smaller than the true ones. This possibility is supported by the fact that the magnitudes of the electro-optic coefficients determined from the scattering efficiences in Ref. 3 are also about 2 times smaller than the directly measured ones.

The antiresonance of the E_{1L} mode at 1.6 eV, and the corresponding negative value of B, must be due to the electro-optic contribution as suggested in Ref. 15, since it does not happen for the E_{1T} phonon. We note that in other wurtzite-type materials (CdS, ZnS) antiresonances have been observed for the transverse modes.[30,31] It is remarkable that no such antiresonances occur in ZnO. We point out that the elastro-optic constants of CdS exhibit an antiresonance as the gap is approached, with a large contribution of the background.[26] The same constants also have an antiresonance in ZnO, but with a much smaller background contribution. This reflects the same trend as the disappearance of antiresonances in the A_{1T}, E_{1T}, and E_2 modes in going from CdS to ZnO.

The second-order resonances of Fig. 6 have been fitted with the second derivative of the dielectric constant according to Eqs. (6) and (7). There is some arbitrariness in this choice: The structure at 208 cm^{-1} can certainly be fitted equally well with Eq. (3). The $2E_{2L}$ resonance, however, can be fitted better with Eq. (6) and thus we assume it is the result of an iterated process involving the Fröhlich interaction.[32] Two iterated first-order processes would also have to be involved for the other

second-order structures if the choice of a second derivative fit proved to be of the essence. A first derivative fit would imply a process involving one single-electron–two-phonon vertex.[32]

Finally, by looking at Fig. 1 we can make a tentative assignment for the second-order structures whose resonance is presented in Fig. 6. The structure at 208 cm^{-1} corresponds to the frequency of $2E_2$ (101 cm^{-1}) at Γ: as shown in Fig. 1 the dispersion relation is very flat around this point. This structure could also contain a contribution of the lower TA branch around the M point; the corresponding K-space multiplicity would enhance this contribution. The peak at 332 cm^{-1} should be ascribed to two phonons from the K-M-Σ around 160 cm^{-1}. Both structures just mentioned are seen in (xx) and (zz) configurations. The structure around 541 cm^{-1} is stronger in the (zz) configuration and corresponds to phonons from the region between the Γ and M points around 270 cm^{-1}. The peak at ~1160 cm^{-1} is known to arise from two LO zone-center phonons.

Note added in proof. We have recently measured (M. H. Grimsditch, private communication) the $A_{1T}(zz)$ mode of ZnO with respect to diamond (6.1×10^{-7} cm^{-1} $sterr^{-1}$, M. H. Grimsditch and A. K. Ramdas, Phys. Rev. B11, 3139 (1975)) and confirmed the original values of Ref. 3. Hence the discrepancy between the two first columns of Table II cannot be attributed to an error in the determination of the absolute cross section. We feel the problem must lie in the oversimplification involved in attributing piezooptical deformation potentials solely to their phonon component.

---

*Supported in part by the Alexander von Humboldt Foundation, on leave from the University Autonoma de Madrid.

[1]W. L. Roth, in *The Physics and Chemistry of II-VI Compounds*, edited by M. Aven and J. S. Prener (North-Holland, Amsterdam, 1967), p. 122.
[2]J. Birman, Phys. Rev. 115, 1493 (1959).
[3]C. A. Arguello, D. L. Rousseau, and S. P. S. Porto, Phys. Rev. 181, 1351 (1969).
[4]A. W. Hewot, Solid State Commun. 8, 187 (1970).
[5]R. Loudon, Adv. Phys. 13, 423 (1964).
[6]K. Thoma, B. Dorner, G. Duesing, and W. Wegener, Solid State Commun. 15, 1111 (1974).
[7]U. Rössler, Phys. Rev. 184, 733 (1969).
[8]S. Bloom and I. Ortenburger, Phys. Status Solidi B 58, 561 (1973).
[9]M. Cardona, *Modulation Spectroscopy* (Academic, New York, 1969), p. 255.
[10]J. O. Dimmock, in *II-VI Semiconducting Compounds*, edited by D. G. Thomas (Benjamin, New York, 1967), p. 277.
[11]See B. Segall, in Ref. 1, p. 67.
[12]See, for instance, M. Cardona, *Light Scattering in Solids*, (Springer-Verlag, Berlin, 1975); and W. Richter, in *Springer Tracts in Modern Physics*, (Springer, Berlin, 1976), Vol. 78.
[13]Y. Oka and T. Kushida, J. Phys. Soc. Jpn. 33, 1372 (1972).
[14]R. Zeyher, Phys. Rev. B 9, 4439 (1974).
[15]R. H. Callender, S. S. Sussman, M. Selders, and R. K. Chang, Phys. Rev. 7, 3788 (1973).
[16]R. C. Miller and W. A. Nordland, Phys. Rev. 132, 4896 (1970).
[17]J. E. Rowe, M. Cardona, and F. H. Pollak, Solid State Commun. 6, 239 (1968).
[18]J. L. Freeouf, Phys. Rev. B 7, 3820 (1973).
[19]D. G. Thomas, J. Phys. Chem. Solids 15, 86 (1960).
[20]R. E. Dietz, J. J. Hopfield, and D. G. Thomas, J. Appl. Phys. 32, 2282 (1961).
[21]T. C. Damen, S. P. S. Porto, and B. Tell, Phys. Rev. 142, 570 (1966).
[22]J. Scott, Phys. Rev. B 2, 1209 (1970).
[23]T. C. Damen, R. C. C. Leite, and J. Shah, in Proceedings of the Tenth International Conference on the Physics of Semiconductors, Cambridge, Mass., 1970 (unpublished).
[24]E. Mollwo, Z. Phys. 6, 257 (1954).
[25]Y. S. Park and J. R. Schneider, J. Appl. Phys. 39, 3049 (1968).
[26]P. Y. Yu and M. Cardona, J. Phys. Chem. Solids 34, 29 (1973).
[27]M. Cardona, in *Atomic Structure and Properties of Solids*, edited by E. Burstein (Academic, New York, 1972), p. 514.
[28]D. W. Langer, R. N. Euwema, K. Era, and T. Koda, Phys. Rev. B 2, 4005 (1970).
[29]R. Martin, Phys. Rev. B 1, 4005 (1970).
[30]J. M. Ralston, R. L. Wadsack, and R. K. Chang, Phys. Rev. Lett. 25, 814 (1970).
[31]R. H. Callender, M. Balkanski, and J. L. Birman, in *Light Scattering in Solids*, edited by M. Balkanski (Flammarion, Paris, 1971), p. 40: J. L. Lewis, R. L. Wadsack, and R. K. Chang, *ibid.*, p. 41.
[32]See for instance, R. L. Schmidt and M. Cardona, Phys. Rev. B 11, 746 (1975).
[33]T. B. Bateman, J. Appl. Phys. 33, 3309 (1962).
[34]R. L. Knell and D. W. Langer, Phys. Lett. 21, 370 (1966).
[35]V. Heine and M. L. Cohen, in *Solid State Physics*, edited by F. Seitz, D. Turbull, and H. Ehrenreich (Academic, New York, 1970), Vol. 24, p. 1.